

Local and Global Mechanical Behavior and Microstructure of Ti6Al4V Parts Built Using Electron Beam Melting Technology



LEILA LADANI

Laser and electron beam melting are prime technologies in metallic powder bed additive manufacturing in which parts are built layer by layer using high energy source. The technology is at a level where each layer can be as thin as 50 μm . Melting and solidification of each powder layer is typically accompanied by some subsurface melting to assure adherence and fusion of layers. In addition to anisotropic mechanical behavior of material caused by layering phenomenon, it is expected that the local mechanical behavior and microstructure vary throughout each build. In this manuscript, local and global mechanical behavior of Ti6Al4V parts produced using electron beam melting technology is investigated using bulk scale mechanical testing and nanoindentation. Parts fabricated in different build orientation were tested at different strain rates at a large scale. The experiment showed that strength is minimal perpendicular to the build plate. Additionally, material exhibited different local mechanical properties relative to distance from base plate. Investigation of the microstructure indicated very distinguished variations in the grain size and alpha and beta phase formation of material in different locations of part relative to build plate. Strength reduction in perpendicular direction is examined and explained through understanding of the microstructure and plastic deformation mechanism in α phase and prior β grains.

DOI: 10.1007/s11661-015-2965-6

© The Minerals, Metals & Materials Society and ASM International 2015

I. INTRODUCTION

A critical issue in additively manufactured parts is whether consistent mechanical properties and microstructure can be achieved. Ti6Al4V is a two-phase Ti alloy which constitutes a very important class of structural metals. The mechanical behavior of these materials can be significantly varied by tailoring their microstructure.^[1] Many different types of microstructures can be obtained through a controlled cooling of this material.^[2] Very slow cooling rate of this material will result in α phase globular in primary β phase grain boundaries.^[2] Small increase in the cooling rate results in formation of α platelets in primary β phase grains. The length of these platelets depends on the cooling rate. As cooling rate increases, at a certain level, a basket-weave type of microstructure forms. Quenching the material will result in the transformation of β into martensitic type α .

Mechanical behavior of this material is strongly influenced by its microstructure.^[3] For example, the existence of globular α phase or platelets enhances the resistance to micro-crack development. The ductility, yield strength (YS), and crack propagation resistance are improved as the size of colonies of platelets

decreases.^[4] Plastic deformation in Ti6Al4V material at room temperature was found to be caused by planar slip in the α grains, at quasi-static strain rates, while at high strain rates deformation twinning is also observed.^[5]

Traditional processes such casting, rolling, or annealing have been studied vastly and their effect on the microstructural formation and mechanical behavior is well understood. Electron and laser melting processes, however, are fairly new and more complicated than traditional techniques. There is less control over the process and many process parameters can affect the outcome. The fact that each layer is built with partial re-melting and solidification of the previous layer and heat extraction occurs in different manners for different geometries adds complexity to the process.

Recent investigations of electron beam melting technology have shown wide variation of microstructure depending on the geometry. Study conducted by Antonyamy^[4] showed favored growth orientation along $\langle 001 \rangle$ β normal to the build plate. It was also found that the grain orientation depends on the sample thickness. In specimens built with larger thickness, the grains were more oriented in $\langle 001 \rangle$ direction, whereas in smaller thickness more random orientation was observed.

Change in mechanical properties relative to distance from build plate were evaluated in an experiment conducted at NIST.^[3] Even though the EBM samples showed a measurable change in the thickness of α platelets as the distance from build plate increased, the

LEILA LADANI, Associate Professor, is with the Mechanical Engineering Department, University of Connecticut, Storrs, CT. Contact e-mail: lladani@enr.uconn.edu

Manuscript submitted December 29, 2014.

Article published online May 20, 2015

tensile test did not show significant variations in mechanical behavior as function of distances from the base plate. The specimens in this case underwent post-process electro-discharge machining (EDM) and micro-hardness tests conducted on the surface that may be skewed due to the heat-affected zone created during the EDM. In another study conducted by the same group, part orientation, melt pool size, and location of the part were investigated. Contradictory to the previous studies^[3,5] which showed the preferential growth orientation along the build direction and anisotropy in mechanical properties, this study did not show significant anisotropy in ultimate tensile strength and YS. Opposite to the findings of Ladani *et al.*^[5] which showed more ductility along the build direction, this study found 30 pct less ductility in that orientation. Both studies showed lower hardness in vertically built parts.

Extensive research on EBM technique, quality of parts, types of defects, process parameter effects on defects, microstructure of material produced using this technique and mechanical behavior of parts over the last decade was conducted by Murr *et al.*^[6-11] One relevant conclusion made by this group was the change in the microstructure due to variation in the heat transfer rate from the bottom to the top of the specimen which caused the variation in microstructure through specimen height and consequently the variation in the hardness values.^[6] This indicates that local mechanical properties may vary through the parts. The global behavior is usually somehow affected by the local properties (*e.g.*, large local defects or weaknesses may cause premature failure of the parts). The idea that heat extraction can be utilized to form the desired microstructure was explored and to some extent realized by Oak Ridge National Lab recently as a structure was built in a carefully controlled manner in which the grain orientation was dictated and controlled at microscale. However, the amount of control that one may have on the process parameters is limited due to the fact that these parameters have a range of practical values. For extreme cases, the geometry may still play a very strong role as it is the prime factor that affects the heat conduction and extraction. As the distance from the base plate increases, the heat extraction is decreased as the thermal resistance increases. The research here presents fabrication, mechanical testing, and microstructural analysis to test this hypothesis.

Additionally, the results presented by most of the researchers, thus far, were on specimens that have been post processed after EBM or laser melting. Post-processes such as EDM or polishing and machining were used to either form the parts to the desired final shape or remove the surface asperities and roughness. However, a major transformational advantage of AM technology is the potential to produce parts to their final net shape without further need for post-processing. This means that in future, parts will be produced using this technology and will be used as produced. Therefore, understanding the mechanical properties of the “*as built*” parts is significant. Therefore, parts that are examined in this study are the “*as built*” parts without further processing.

II. FABRICATION

Dog-bone specimens are fabricated based on the E8 M-04 ASME standard for subsize specimen using EBM system, Arcam[®] A2 manufactured by Arcam[®] AB in Sweden.^[13] The Computer-Aided Design (CAD) dimensions of the parts are $100 \times 10 \times 3$ mm with a gage length of 25 mm. The subsize specimen is selected due to the limited mechanical testing capability and the thickness is reduced accordingly to 3 mm. The specimens were fabricated in three different build orientations with respect to the build table as seen in Figure 1. In the top-built samples, the layers are stacked in longitudinal direction. In the side-built samples, the layers are stacked in the width direction and in the flat-built samples, the layers are stacked through the thickness.

The particle size used in fabrication was on average 0.07 mm. Powder layer thickness was 0.07 and 0.069 mm after melt. Beam size was $500 \mu\text{m}$. For quality electron beam, the upper chamber is kept at 7.5×10^{-7} Torr. (1 Torr = 0.00131578947 atm) and to avoid oxidation of titanium, the fabrication chamber maintained a pressure of 7.5×10^{-5} Torr.^[13]

III. MECHANICAL BEHAVIOR

A. Bulk Behavior

Mechanical testing at bulk level was conducted using an electromechanical tensile tester and strain was measured at the gage region using extensometer. The test was conducted in three different strain rates of 0.0005, 0.001, and 0.01 S^{-1} . True stress–strain and engineering stress–strain data are extracted from the tests. Six to seven specimens in each build direction were tested. Average stress–strain curves are plotted in Figure 2. As seen in this figure, regardless of strain rate, flat-built samples generally show higher strength and better properties. Top-built samples have the smallest strength, but show higher ductility than other two build directions. The properties obtained using

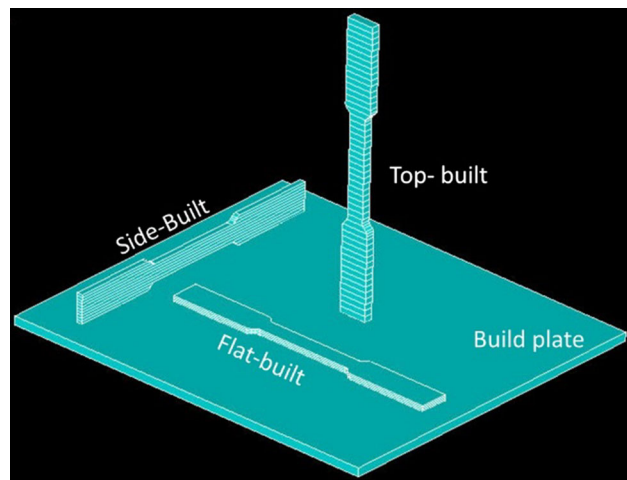


Fig. 1—Dog-bone samples fabricated using the Arcam machine in three different orientations with respect to the build table.

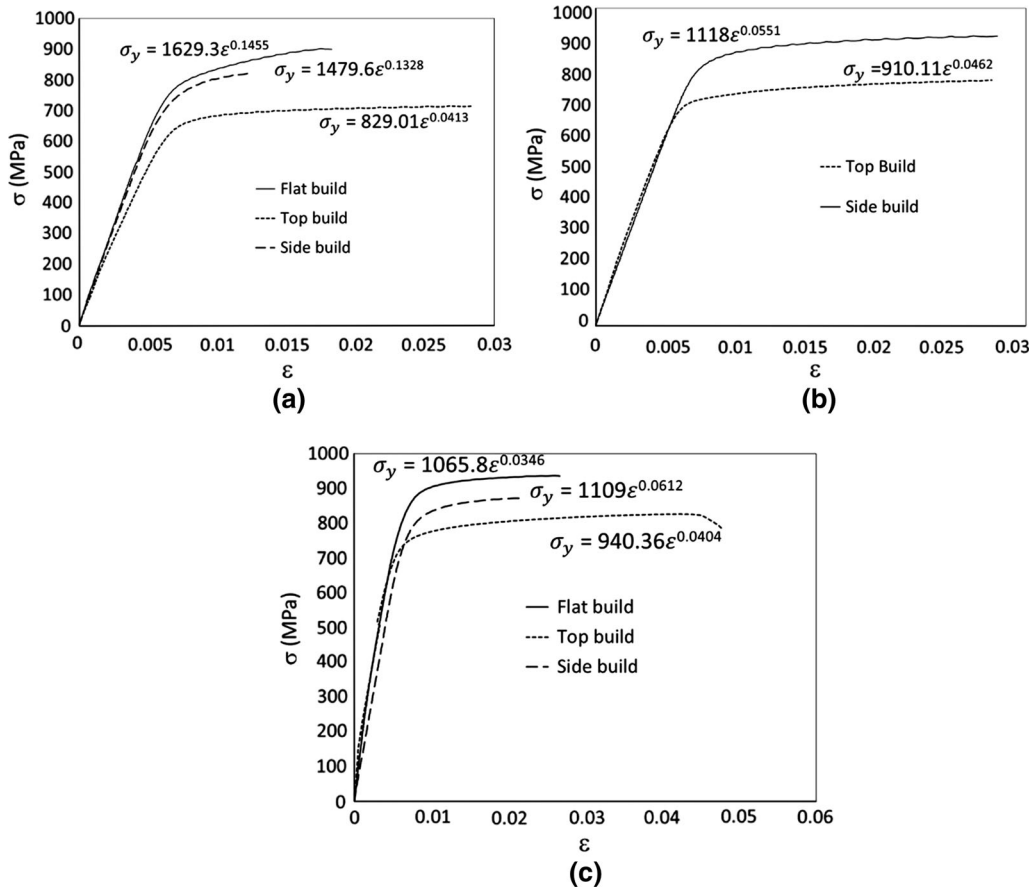


Fig. 2—Comparison of stress–strain data for different build orientations. (a) Strain rate of 0.0005 S^{-1} , (b) strain rate of 0.001 S^{-1} , and (c) strain rate of 0.01 S^{-1} .

these specimens were close to the properties of Ti6Al4V material fabricated using traditional techniques and also comparable to the other tests conducted on EBM post-processed samples.^[14–17]

Looking closer at the plastic region and flow stress of the material, a power-law equation can be fit to represent flow stress as a function of plastic strain and obtain the hardening exponent as seen in Figure 2. It can be clearly seen from these figures that the average hardening exponent is a function of the strain rate. However, very interestingly, the strain hardening exponent in top-built samples is independent of the strain rate and is about 0.04 in all strain rates. However, for flat-built and side-built samples, the strain hardening exponent decreases as the strain rate increases from 0.0005 to 0.01. Hardening exponent is larger in side-built and flat-built samples in very low strain rate. The low values of hardening exponent are believed to be caused by the limited number of mechanisms and mainly due to the planar slip of the primary α phase.^[14]

In uniaxial tensile/compressive testing, strain rate sensitivity (SRS) is measured as the change in observed strength as the applied strain rate is varied. SRS is often represented using the following equation:^[13]

$$m_{\text{uniaxial}} = \frac{d(\ln(\sigma))}{d(\ln(\dot{\epsilon}))}, \quad [1]$$

where m is SRS exponent in

$$\sigma = k(\dot{\epsilon})^m. \quad [2]$$

Traditionally manufactured Ti6Al4V has shown strong positive SRS in literature.^[12] A similar behavior is observed in top-built material in this experiment. Positive strain rate manifests itself in higher strength at higher strain rates. The side-built and flat-built samples did not show a distinguished SRS behavior. The values of m and k are calculated at 1 pct strain for top-built orientation and are 6.83 and 0.0374, respectively.

B. Local Behavior

The variation of properties shown in different orientations could be caused by several factors such as variation in microstructure, change in grain size, variation of microstructural features such as α and β colony sizes, platelet thickness or grain orientation, increased level of defects, or surface asperities. Top-built samples are made from many more layers than the side-built and flat-built samples which could increase the probability of getting defects in between the layers. Additionally more surface asperities and defects are expected in top-built samples.

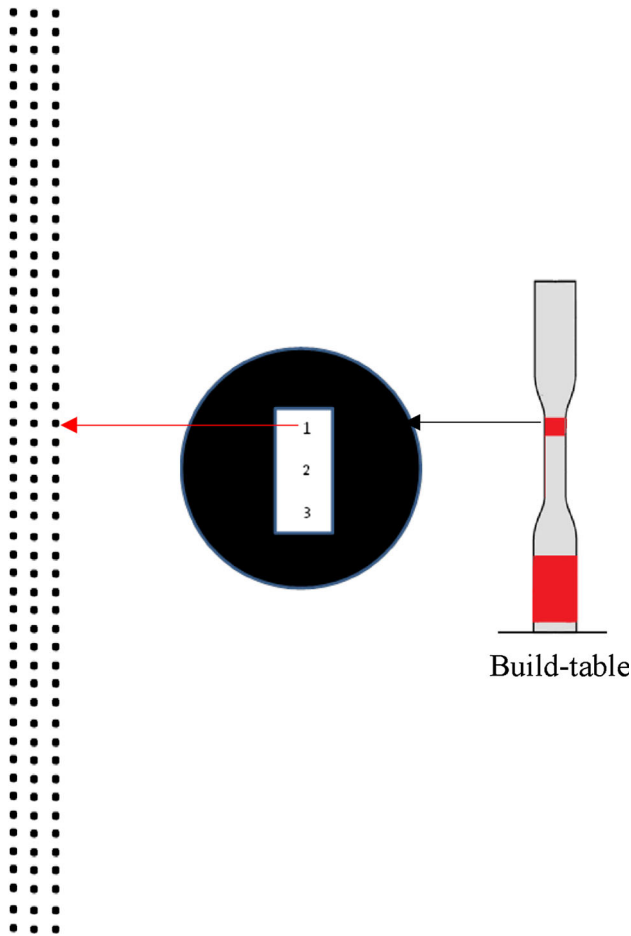


Fig. 3—Nanoindentation procedure.

As the microstructure varies, so the mechanical behavior. To evaluate the variation of microstructure and mechanical behavior throughout the build, nanoindentation was performed on top-built sample at the bottom and top of the samples as shown in Figure 3. Two different places on the specimen were selected as seen in this figure to compare the effect of distance from build table. Three nanoindentation tests were performed on each location. Each test consisted of a pattern of 3×50 indents with $5 \mu\text{m}$ distance. The pattern was selected such that indentations can be across the layers, and interfaces of layers and direct comparison can be made in indentation response.

Almost 130 to 150 indents were done at each position on all the specimens. The program was set to indent 150 points for each run of the test. Outliers were discarded. Hardness was calculated using the nanoindentation load-displacement curve. A comparison between top and bottom sections of the top-built sample are shown in Figure 4. Murr *et al.* have reported the average micro-indentation hardness ranges from 3.6 to 3.9 GPa.^[7] Li *et al.* have found that the average nanoindentation hardness values lie in between 4-5 GPa.^[18] Qian *et al.* have found that nanoindentation hardness values are 10 to 30 pct higher than the micro-indentation hardness values for the same samples.^[19] The average

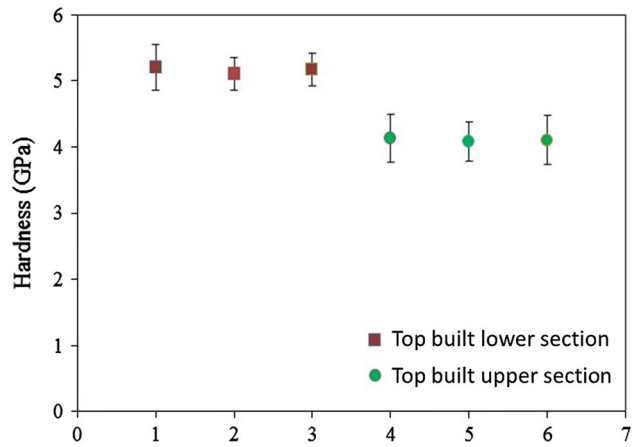


Fig. 4—Comparison of hardness between two sections of top-built sample.

value of hardness for the top-built sample is found to be 4.11 for the top section and 5.6 for the bottom section. The top portion of the top-built sample shows almost 20 pct less hardness than its bottom portion as seen in Figure 4. This feature can be attributed to the microstructure difference as it differs due to the cooling rate. Since the build table remains at about 1123 K (850°C) while the melting occurs above 1155 K (882°C), the temperature gradient is higher close to the build table. Heat that is conducted to the surrounding insulator powder does not significantly compare to the heat that is conducted toward the build table. Thus the solidification rate at bottom is higher that leads to finer α -plates while the slower solidification rate at the top region leads to coarse α -plates.^[16] The analysis of the microstructure as followed here in the next section shows that this hypothesis is correct.

IV. MICROSTRUCTURAL ANALYSIS

To evaluate the anisotropic formation of grains and microstructure, samples from side-built, top-built, and flat-built were cross sectioned and polished. The sections were all taken perpendicular to the length of the dog-bone samples. Therefore, in the side-built and flat-built samples, these sections have multiple layers while in top-built sample, the section was taken parallel to the build layers which theoretically means that it is through one layer. Sections were polished using aluminum oxide slurry and etched using Kroll's etchant with distilled water, and hydrofluoric and nitric acids. Optical microscope and scanning electron microscopy images were taken from the sections before and after etching.

Perhaps the most interesting observation that also confirms the findings of the previous studies is that in side- and flat-built samples, the grains can be seen to have grown vertically perpendicular to the build orientation as seen in Figure 5(b).^[3] These indicate the prior β grains which contain the α colonies that start to form at the grain boundaries and move inward into β grains. There is a slight angle between the growth of these prior

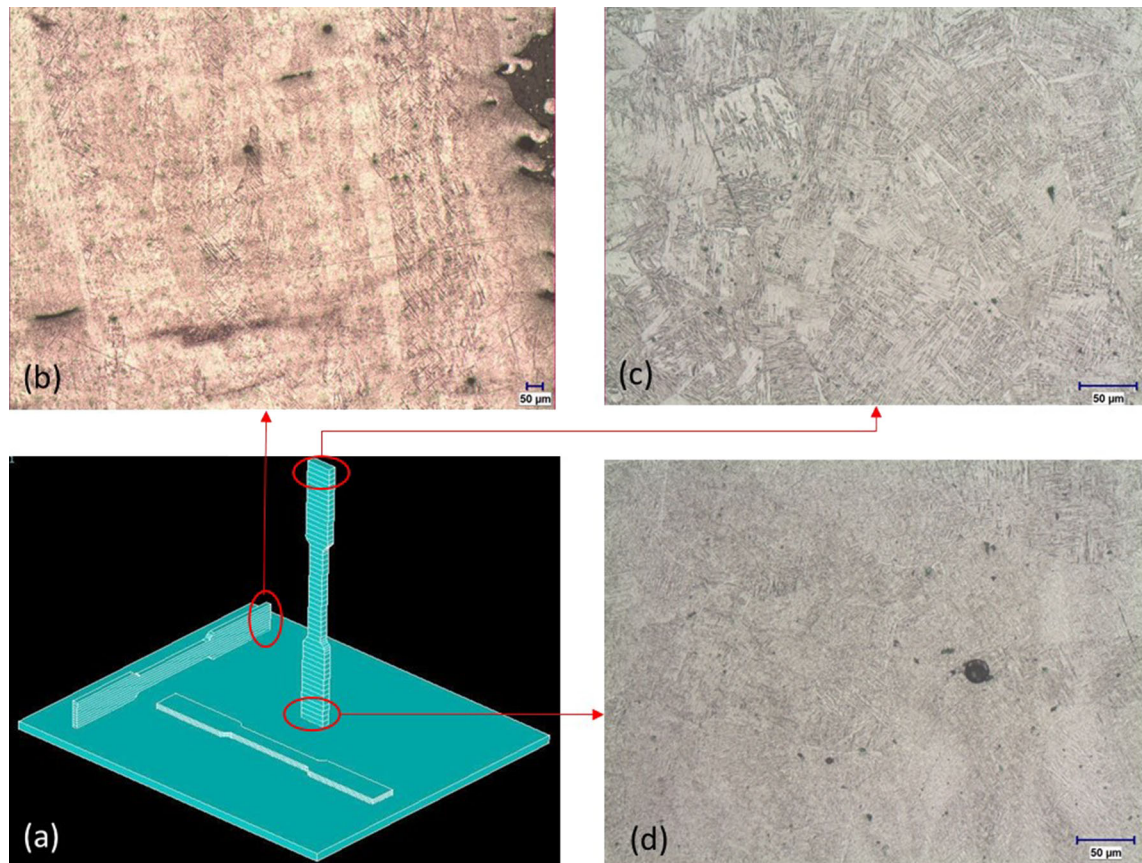


Fig. 5—(a) Cad model of the different build orientation and illustration of the sections taken for microstructural analysis, (b) optical microscope image of the side-built sample, (c) optical image of the top of the top-built section, (d) optical image of the bottom of the top-built section.

β grains and the build orientation. This is basically the direction of the highest temperature gradient as the beam moves. The same trend follows for side-built samples. Grain boundaries appear to be columnar and follow the build layer direction upward.

However, for the top-built samples, it can be seen that both alpha and beta phases are uniformly dispersed and no columnar grain growth behavior is apparent. A comparison between the section taken on top of the sample versus the one taken from the bottom of the sample in top-built sample shows significant difference in the size of the grains and platelets. On the bottom face, which is the face that is close to the build table, grains are large having refined basket-weave platelet structures. The top surface, however, has smaller grains having extremely coarse basket-weave structures and thick platelets as seen in Figures 5((c) and (d)) and 6.

The columnar growth of the grains along the build direction can be the reason for anisotropic behavior in both elastic and plastic regions. For the side-built and flat-built specimens, the tensile load direction is perpendicular to the columnar growth direction. With the stress axis perpendicular to the columnar prior β -grains, deformation may become highly localized in columnar grains inhabited by the weaker colonies. The main hardening cause is dislocation pile up at the grain boundaries. In a case where the prior β grain boundaries

are perpendicular to the loading direction, the dislocations may not have a long distance to travel. Additionally, existence of the α platelets limits the motion of dislocation along these platelets.^[20]

At room temperature, the HCP structure of the α phase is the dominant factor in determining the anisotropic deformation of Ti6Al4V. This anisotropic deformation can manifest in both elastic and plastic regions. In a mechanical testing of a single crystal α phase Ti6Al4V, the elastic modulus was found to be 145 GPa in the direction of c-axis of the HCP crystal whereas in perpendicular direction to c-axis, it was found to be 100 GPa. In plastic region, the anisotropy manifests itself by activation of different slip systems. Critical resolved shear stress is found to be minimum for the basal and prismatic planes in α phase Ti6Al4V. β phase, however, acts more uniformly in different orientations due to its BCC crystal structure. β and α phase each has different number of slip systems and the grain orientation will dictate how the stresses are resolved on these slip systems resulting in shearing and slip. As this study suggests and has been shown by several other studies, additively manufactured parts typically experience columnar growth parallel to the build direction^[21] with prior β grain boundaries along the build direction. α platelets typically start at the prior β grain boundaries and grow inward with a certain angle as shown in the

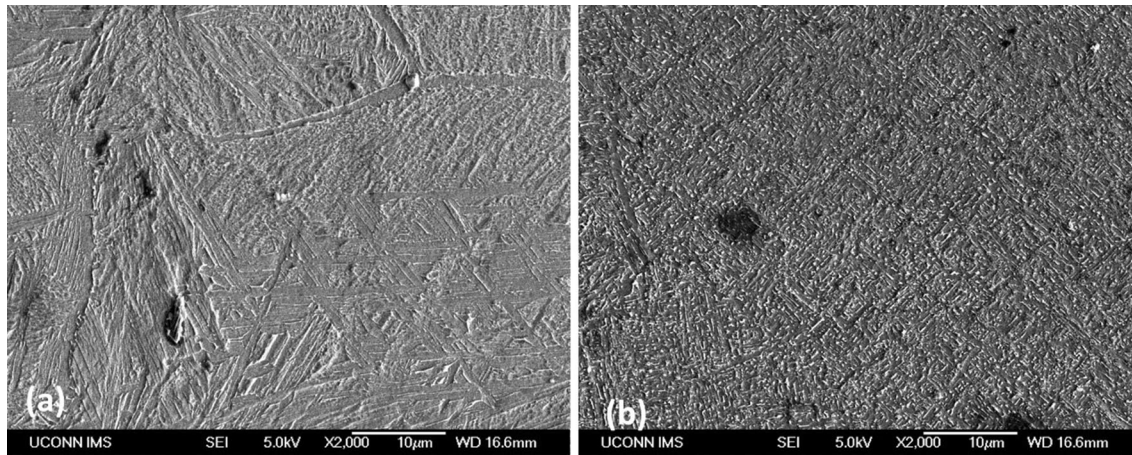


Fig. 6—SEM images of etched specimens (a) top of the top-built samples, (b) bottom of the top-built sample.

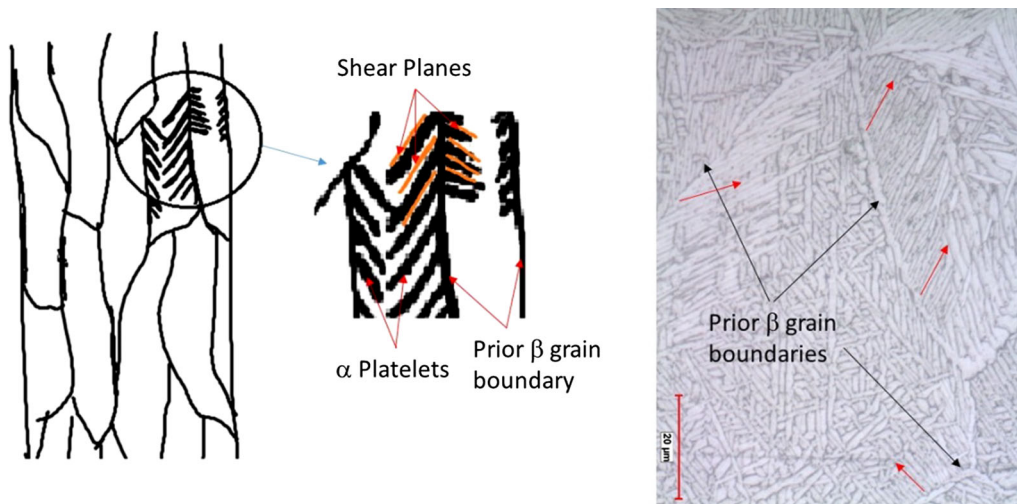


Fig. 7—Schematic illustration of $(\alpha + \beta)$ and likely shear planes at the interface of α and β . The micrograph shows the prior β grain boundaries and α platelets growth direction.

micrograph in Figure 7. It is previously shown that the dislocation glide can occur easily at shallow angles with respect to lamellar $(\alpha + \beta)$ interface as opposed to large angles. At large angles, the slip length is shorter. Additionally, it is much harder for slip transition to occur across α and β interface. It was also shown in an in situ mechanical testing of these parts the most active slip planes were the planes parallel to the α platelets.^[21] Naturally, it is also hard for the slip transition to occur at the grain boundary between two prior β grains due to difference in the crystal orientation and noncolinearity of slip planes. In other words, the shearing typically occurs mostly along α platelets and stops at prior β grain boundaries as schematically shown in Figure 7.

In top-built samples, the long prior β grains are oriented along the loading direction. Consequently, the texture of the grains allow summation of slips in the loading direction thereby allowing more plastic deformation before failure. In loading perpendicular to the columnar direction, the deformation is limited by the

grain boundaries and therefore, the side-built and flat-built samples show lower ductility.

V. CONCLUSIONS

Local and global mechanical testing are conducted on Ti6Al4V specimens built in different orientations using electron beam melting technology. Tensile tests conducted on the “*as build*” samples showed lower strength in specimens built perpendicular to the build table. These specimens also showed lower hardness in the nanoindentation tests. Evaluation of local mechanical properties and microstructure of the specimens built perpendicular to the build table shows that as the layers are built, the microstructure varies with smaller grain sizes and larger platelet thickness as the distance to build table increases. The hardness values obtained showed lower values for the specimens closer to the build table.

Plastic behavior shows anisotropic trend as the hardening exponent seems to be independent of the strain rate in specimens built perpendicular to the build table. However, specimens built sideway or flat showed larger strain hardening exponent at higher strain rates. On the other hand, the specimens built perpendicular to the build table showed positive SRS while other two orientations showed no trend. Microstructural orientation analysis showed columnar β grain growth in the orientation perpendicular to the build table. Anisotropic plastic behavior of the samples is theoretically related to this columnar growth and the preferred slip planes at the α and β interface.

REFERENCES

1. J. Sieniawski, and W. Ziaja: *Titanium Alloys—Advances in Properties Control*, ISBN 978-953-51-1110-8, Published: May 15, 2013 under CC BY 3.0 license. ©The Author(s).
2. R. Pederson: Thesis, Luena University of Technology, 2002.
3. J.W. Foltz, B. Welk, P.C. Collins, H.L. Fraser, and J.C. Williams: *Metall. Mater. Trans. A*, 2011, vol. 42A, pp. 645–50.
4. P.S. Follansbee and G.T. Gray, III: *Metall. Trans. A*, 1989, vol. 20, pp. 863–74.
5. A. Antonysamy, J. Meyer, and P.B. Prangnell: *Mater. Charact.*, 2013, vol. 84, pp. 153–68.
6. L. Ladani, J. Razmi, and S.F. Choudhury: *J. Eng. Mater. Technol.*, 2014, vol. 136 (3), pp. 031006-1–031006-7.
7. L.E. Murr, E.V. Esquivel, S.A. Quinones, S.M. Gaytan, M.I. Lopez, E.Y. Martinez, F. Medina, D.H. Hernandez, E. Martinez, J.L. Martinez, S.W. Stafford, D.K. Brown, T. Hoppe, W. Meyers, U. Lindhe, and R.B. Wicker: *Mater. Charact.*, 2009, vol. 60, pp. 96–105.
8. L.E. Murr, S.M. Gaytan, F. Medina, E. Martinez, D.H. Hernandez, L. Martinez, M.I. Lopez, R.B. Wicker, and S. Collins: *Solid Freeform Fabr. Symp. Proc.*, 2009, pp. 374–97.
9. L.E. Murr, S.A. Quinones, S.M. Gaytan, M.I. Lopez, A. Rodela, E.Y. Martinez, D.H. Hernandez, E. Martinez, F. Medina, and R.B. Wicker: *Mech. Behav. Biomed. Mater.*, 2009, vol. 2, pp. 20–32.
10. S.M. Gaytan, L.E. Murr, F. Medina, E. Martinez, M.I. Lopez, and R.B. Wicker: *Mater. Technol.*, 2009, vol. 24, pp. 180–90.
11. L.E. Murr, E. Martinez, S.M. Gaytan, D.A. Ramirez, B.I. Machado, P.W. Shindo, J.L. Martinez, F. Medina, J. Wooten, D. Ciscel, U. Ackelid, and R.B. Wicker: *Metall. Mater. Trans. A*, 2011, vol. 42A, pp. 3491–3508.
12. L.E. Murr, S.M. Gaytan, A. Ceylan, E. Martinez, J.L. Martinez, D.H. Hernandez, B.I. Machado, D.A. Ramirez, F. Medina, and S. Collins: *Acta Mater.*, 2010, vol. 58 (5), pp. 1887–94.
13. E. Rawn: “Oak Ridge National Laboratory Develops 3D Printing Process at the Microscale”, 2014. ArchDaily. Accessed 21 Dec 2014. <http://www.archdaily.com/?p=566979>.
14. <http://www.arcam.com/CommonResources/Files/www.arcam.com/Documents/EBM%20Materials/Arcam-Ti6Al4V-Titanium-Alloy.pdf>.
15. U. Lindhe, O.L. Harrysson: *Solid Freeform Fabrication Symposium Proceedings*, 2003, pp. 433–38.
16. J.R. Schroeder: *Advanced Manufacturing Technology Changes the Way Implants are Designed and Produced*. Fall, BONEZone, 2006, pp. 17–20.
17. S. Thundal: *Adv. Mater. Process*, 2008, vol. 166, pp. 60–62.
18. V. Maier, K. Durst, J. Mueller, B. Backes, H.W. Höppel, and M. Göken: *J. Mater. Res.*, 2011, vol. 26, pp. 1421–30.
19. R. Li, L. Riesterb, T.R. Watkins, P.J. Blaub, and A.J. Shih: *J. Mater. Sci. Eng. A*, 2008, vol. 472, pp. 115–24.
20. L. Qiana, M. Lib, Z. Zhoua, H. Yanga, and X. Shia: *Surf. Coat. Technol.*, 2005, vol. 195 (2–3), pp. 264–71.
21. M.B. Mathisen: Norwegian University of Science and Technology, Master Thesis, 2012.